Li self-diffusion in garnet-type $Li_7La_3Zr_2O_{12}$ as probed directly by diffusion-induced ^7Li spin-lattice relaxation NMR spectroscopy

A. Kuhn,[1] S. Narayanan,[2] L. Spencer,[3] G. Goward,[3] V. Thangadurai,[2] and M. Wilkening[1,*]

[1]*Institute of Physical Chemistry and Electrochemistry, Leibniz University Hannover, Callinstr. 3a, D-30167 Hannover, Germany*

[2]*Department of Chemistry, University of Calgary, 2500 University Drive NW, Calgary, Alberta, Canada T2N 1N4*

[3]*Department of Chemistry, McMaster University, 1280 Main Street W, Hamilton, Ontario, Canada L8S 4M1*

(Received 18 November 2010; published 15 March 2011)

Li self-diffusion in garnet-type $Li_7La_3Zr_2O_{12}$, crystallizing with tetragonal symmetry at room temperature, is measured by temperature-variable ^7Li spin-spin as well as spin-lattice relaxation (SLR) nuclear magnetic resonance (NMR) spectroscopy. The SLR NMR rates which were recorded in both the laboratory and the rotating frame of reference pass through characteristic diffusion-induced rate peaks allowing for the direct determination of Li jump rates τ^{-1}, which can be directly converted into self-diffusion coefficients D_{sd}. The NMR results are compared with those obtained from electrical impedance spectroscopy measurements carried out in a large temperature and wide frequency range. Taken together, the long-range diffusion process, being mainly responsible for ionic conduction at ambient temperature, is characterized by an activation energy of approximately 0.5 eV, with $\tau_0^{-1} \approx 1 \times 10^{14}$ s^{-1} being the pre-exponential factor of the underlying Arrhenius relation.

DOI: 10.1103/PhysRevB.83.094302 PACS number(s): 66.30.−h, 76.60.−k, 82.56.−b, 82.47.Aa

I. INTRODUCTION

Crystalline solids with a high Li-ion conductivity[1–5] but a vanishing electronic conductivity are of great importance in current developments of new chemically resistant electrolytes. Such materials are urgently needed in the field of clean and safe energy storage systems such as powerful supercapacitors as well as advanced high-energy density lithium-ion batteries.[6–10] Recently, garnet-type $Li_7La_3Zr_2O_{12}$ crystallizing with cubic symmetry[11] has attracted great attention[9,10,12] because of its high ionic conductivity.[11] At room temperature the bulk conductivity of a sample with cubic symmetry is reported to be high enough to make the development of all-solid-state Li-ion batteries feasible.[11,12] The tetragonal phase of $Li_7La_3Zr_2O_{12}$ shows an Li-ion conductivity in the order of 10^{-6} S cm^{-1} at ambient temperature.[13] This value is comparable to that of most oxide ceramics belonging to the group of good Li-ion-conducting solids, which includes also those of the large family of structurally complex garnet-type compounds studied during the past years.[2,9,10,14–19]

So far, Li transport properties in garnets of the composition $Li_7La_3Zr_2O_{12}$, as well as others,[9] have been exclusively studied by (alternating-current) impedance spectroscopy.[11–13] Alternatively, Li nuclear magnetic resonance (NMR) techniques[20–28] can be used to provide direct insights into Li dynamics and to quantify the ion diffusivity in solids precisely over a large dynamic range.[29–32] NMR is a nondestructive and noncontact method, making it advantageous over other techniques capable of studying ion dynamics. For example, no elaborate postpreparation of the samples including sintering procedures to minimize influences of, for example, blocking grain boundaries, or the application of electrodes, as in the case of impedance spectroscopy, are necessary when NMR techniques are used.

Although a huge number of NMR studies have been published dealing with Li diffusion properties in solids, to our knowledge, only few studies[33–36] employing NMR spectroscopy to probe structural as well as diffusion parameters in Li-containing garnets can be found in the literature. While Koch and Vogel[34] used ^7Li stimulated-echo NMR spectroscopy to trace slow Li dynamics in garnet-type $Li_5La_3Nb_2O_{12}$, van Wüllen *et al.*[33] took advantage of ^6Li 2D exchange NMR spectroscopy to reveal details on the migration mechanism in the same sample. Such investigations are indispensable in order to determine local Li environments, as well as to enlighten the origins of fast Li dynamics in solids. Additionally, the reliable measurement of Li self-diffusion parameters from a microscopic point of view, as it is possible in the case of most of the NMR techniques,[21] provides valuable information to help identify as well as purposefully modify those candidates having the potential to be used as solid electrolytes.

In the case of $Li_7La_3Zr_2O_{12}$ [space group $I4_1/acd$ (tetragonal phase),[13] $Ia\bar{3}d$ (cubic phase)[37]], Li spin-lattice relaxation (SLR) NMR relaxation experiments (see, e.g., Refs. 20,21 and 38–45) are ideally suited to probe Li jump rates which can be directly converted into Li self-diffusion coefficients by applying the Einstein-Smoluchowski equation.[21,32,46–48] In the present contribution, purely diffusion-induced ^7Li SLR NMR rates of $Li_7La_3Zr_2O_{12}$ in both the laboratory and rotating frame of reference were recorded over a large temperature range. The sample studied shows tetragonal symmetry at room temperature. The NMR results are comprehensively compared with those obtained from electrical impedance spectroscopy measurements, leading to a consistent picture of Li dynamics in highly pure $Li_7La_3Zr_2O_{12}$.

II. EXPERIMENT

Tetragonal $Li_7La_3Zr_2O_{12}$ was prepared by conventional solid-state reaction. Stoichiometric amounts of the starting materials (Li_2CO_3, La_2O_3, and ZrO_2) were mixed, put in an alumina crucible, and heated at 1173 K in air for 24 h. An excess (10 wt%) of Li_2CO_3 was added to compensate for any loss of lithium due to volatilization. After that, the mixture was air-quenched and analyzed by x-ray powder diffraction (XRPD) using a D8 Advance diffractometer (Bruker) operating

with Cu K_α radiation at 40 kV and 40 mA (see Fig. 1). Some XRPD patterns were recorded *in situ* using a high-temperature cell HTK-1200N (Anton-Paar) at elevated temperatures. For the NMR measurements performed under static conditions the polycrystalline sample was fire-sealed in quartz tubes under vacuum.

^{6}Li magic angle spinning (MAS) NMR spectra (Fig. 2) as a function of delay time were recorded with a single-pulse experiment. For that purpose an Avance III NMR spectrometer (Bruker) connected to a precisely shimmed cryomagnet with a magnetic field of 14.1 T was used. The field strength corresponds to a resonance frequency of approximately 88 MHz. A standard MAS NMR probe (2.3-mm rotors) was employed. The spinning frequency $\nu_{\rm rot}$ was 30 kHz. As in the case of the ^{7}Li NMR data, a single room-temperature ^{6}Li NMR SLR rate was estimated with the help of a saturation recovery experiment.[21,49] For comparison, some ^{6}Li MAS NMR spectra were recorded at 73 MHz and $\nu_{\rm rot} = 39$ kHz. The spectra shown in Fig. 2 were referenced to 1 M LiCl.

^{7}Li SLR NMR rates in both the laboratory as well as the rotating frame of Refs. 21 and 49 were recorded with an MSL 100 spectrometer (Bruker) which is connected to an Oxford cryomagnet with a magnetic field of 4.7 T. This corresponds to a ^{7}Li resonance frequency of 77 MHz. A standard probe as well as a home-built high-temperature probe were used for the ^{7}Li SLR NMR measurement. The temperature in the sample chamber was monitored by an Oxford ITC4 with an accuracy of about ± 0.5 K. The ITC controls the output of a heater placed inside the probe and its interplay with a stream of either freshly evaporated nitrogen or ambient air. Additional ^{7}Li SLR NMR measurements were carried out using an MSL 400 spectrometer with the same setup and at a resonance frequency of 155 MHz (9.4 T). ^{7}Li SLR times (T_1) were recorded using the saturation recovery pulse sequence.[21,49] Analogous measurements in the rotating frame of reference ($T_{1\varrho}$) were acquired with the spin-lock technique[49] at a locking frequency of $\omega_1/2\pi \approx 30$ kHz. The recycle delay was at least $5T_1$. In both cases the transients were fitted with stretched exponentials. Presumably, such a time behavior is an indication of coupling

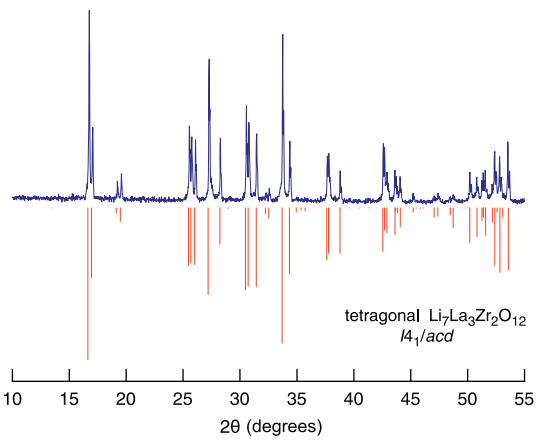

FIG. 1. (Color online) XRPD of $Li_7La_3Zr_2O_{12}$ proving its tetragonal symmetry at room temperature. Vertical lines indicate intensities and diffraction angles calculated on the basis of the neutron diffraction study of Awaka *et al.* (Ref. 13).

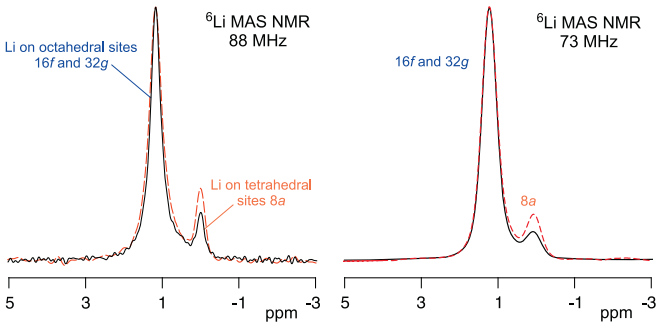

FIG. 2. (Color online) (Left) ^{6}Li MAS NMR spectrum of garnet-type $Li_7La_3Zr_2O_{12}$ recorded at $\nu_{\rm rot} = 30$ kHz and a resonance frequency of 88 MHz. The solid line shows a spectrum obtained from 16 scans which were accumulated at an interval of 2400 s; for the second spectrum (dashed line) 12 scans were accumulated and the delay time was set to 9000 s so that full ^{6}Li NMR SLR is ensured (see text). The main signal can be attributed to Li ions occupying the distorted octahedral sites 16f and 32g. The signal with much lower intensity reflects Li ions residing in the tetrahedral interstices. (Right) ^{6}Li MAS NMR recorded with the same relaxation delays but at 73 MHz and $\nu_{\rm rot} = 39$ kHz. Up to 64 scans were accumulated.

of the hopping Li ions with paramagnetic impurities. ^{7}Li NMR spectra (155 MHz) were obtained by Fourier transformation of the free induction decays (FIDs) measured with a 90° pulse applying the quadrature detection technique.[49] Additionally, (fully relaxed) ^{7}Li-stimulated echo (here spin-alignment echo) NMR spectra were recorded at the same frequency with the Jeener-Broekaert pulse sequence[20,24,50–52] in order to enhance the NMR signal of satellite intensities. Up to 512 scans were accumulated to obtain a satisfying signal-to-noise ratio. Mixing and preparation time were chosen as short as possible.[53]

Li-ion conductivities were measured with a Novocontrol impedance spectrometer which is equipped with a BDS 1200-sample cell and a Beta analyzer (Novocontrol). The latter is capable of measuring impedances down to 10^{-14} S at frequencies ranging from a few μHz to 20 MHz. Temperature regulation and controlling within an accuracy of about 0.5 K was carried out with a Quattro cryosystem (Novocontrol) using dry nitrogen gas. The root-mean-square ac voltage was typically 0.1 to 1.0 V. Prior to the measurements the powder samples were uniaxially cold pressed at 1 GPa to cylindrical pellets (8 mm in diameter and ca. 1 mm in thickness). The thickness of each pellet was measured with a vernier caliper. Electrodes were applied either by Au evaporation using an Edwards 306 or by pressing the uncoated pellet between Pt powder according to a sandwich configuration.

III. RESULTS AND DISCUSSION

A. Characterization of the sample by ^{6}Li MAS NMR

Prior to the temperature-variable NMR measurements, the as-prepared sample was characterized by XRPD as well as (high-resolution) ^{6}Li MAS NMR spectroscopy carried out at ambient bearing gas pressure corresponding to approximately 308 K. It shows the typical XRPD pattern of phase-pure tetragonal $Li_7La_3Zr_2O_{12}$ (Fig. 1), as shown in Ref. 13. Similar to a very recently published study[37] on $Li_7La_3Zr_2O_{12}$, which motivated us to carry out some additional *in situ* XPRD

measurements, the crystal structure slightly changes and the symmetry gradually increases from tetragonal to cubic at elevated temperatures. Whereas in Ref. 37 the transformation starts at approximately 400 K, in the present study it is shifted by almost 200 K toward higher T. Presumably, this reflects the higher purity of the sample investigated here. $Li_7La_3Zr_2O_{12}$ showing purely cubic symmetry is expected to be formed at temperatures larger than 623 K in the present case. However, as we show below, these gradual changes in local structure seem to have almost no effect on the Li jump rates measured, which strictly follow Arrhenius behavior over a wide dynamic range.

The room-temperature ^{6}Li MAS NMR spectra shown in Fig. 2 are dominated by a signal which can be attributed to Li ions on the distorted octahedral interstices 16f and 32g in the garnet-related-type structure of tetragonal $Li_7La_3Zr_2O_{12}$. Only at sufficiently long delay times does a second component show up which is shifted to negative ppm values by about 1.2 ppm (see Fig. 2). The signal with low intensity can be attributed to Li ions occupying the tetrahedral 8a sites in the tetragonal garnet. In the case of a fully relaxed spectrum recorded at a delay time of 9000 s, the corresponding area fraction is approximately 14(1)% of that of the total area. This is in perfect agreement with the crystal structure proposed by Awaka *et al.*[13] The 8a sites are fully occupied by Li ions; i.e., 14.3% of the Li ions reside on tetrahedral interstices.[13] The assignment of the two signals is also consistent with that reported by van Wüllen *et al.*[33] who observed two ^{6}Li NMR signals for $Li_5La_3Nb_2O_{12}$ having a related structure to tetragonal $Li_7La_3Zr_2O_{12}$. Since the two components are well separated, two individual ^{6}Li SLR times T_1 can be measured. Interestingly, T_1 of the main component is approximately 5 s at 88 MHz, whereas that of the other component is on the order of at least 1200 s at 308 K. Thus, from a dynamic point of view the two spin reservoirs are also well separated (cf. Refs. 33 and 36). At room temperature the Li ions representing the minor component are much less mobile than those residing on the octahedral sites. This is in good agreement with the result of van Wüllen *et al.* who analyzed ^{6}Li 2D exchange NMR spectra.[33] Provided these features do not change much with increasing temperature,[54] in the case of the ^{7}Li NMR SLR rate measurements presented below, the rates are exclusively determined by the fast Li ions on the octahedral positions. This is due to the circumstance that the rates were recorded using delay times of up to $5T_1 = 200$ s (at 230 K; see below). For comparison, at 77 MHz the ^{7}Li SLR NMR time turned out to be 2.4 s (308 K), indicating that the diffusion-controlled relaxation mechanism, when probed at ambient temperature, is mainly of dipolar nature for which $T_1(^7\mathrm{Li})/T_1(^6\mathrm{Li}) \approx 1/2$ is expected (see, e.g., Ref. 55 for an analogous estimation).

B. Temperature-variable (static) ^{7}Li NMR spectra

Simultaneously with the measurements of ^{7}Li SLR NMR rates (see below) we have recorded ^{7}Li NMR spectra (Fig. 3) under static conditions and over a wide temperature range. They provide rough information on the diffusion parameters controlling Li hopping at low temperatures in phase-pure $Li_7La_3Zr_2O_{12}$. Moreover, when a larger temperature range is regarded they might provide information on possible structural changes upon heating. The complete ^{7}Li (spin-quantum number $I = 3/2$) NMR line of a powdered sample consists of two components, viz. a first-order quadrupole distributed satellite contribution ($\pm 3/2 \leftrightarrow \pm 1/2$) and the central one ($1/2 \leftrightarrow -1/2$), which is only broadened by nuclear dipole interactions of the spins. At first, the focus is directed toward the central transition of the Li NMR spectra. Satellite intensities, are expected if the ^{7}Li nuclei are placed in sites with a nonvanishing electric field gradient. Such contributions, if they span a wide range of frequencies corresponding to a large quadrupole coupling constant, can be made visible by using suitable NMR echo techniques (see the spectra labeled (a), (b) and (c) shown in the insets of Fig. 3). Satellite intensities are difficult to detect when the spectra are simply obtained by Fourier transformation of the free induction decays (main spectra of Fig. 3). These difficulties are simply caused by receiver dead time effects cutting off sharply decaying components at the initial part of the FID.

1. ^{7}Li NMR spectra: Central lines

Below 260 K the shape of the dipolarly broadened ^{7}Li NMR central line is Gaussian-like and shows a width (full width at half maximum) of approximately 8.6 kHz. This value represents the so-called rigid lattice line width δ_0; in this regime Li motions are characterized by jump rates much smaller than 10^3 s^{-1}. With increasing Li motions ^{7}Li-^{7}Li dipole-dipole interactions are increasingly averaged, resulting in a narrowing of the width δ which is already decreased to 1.2 kHz when T reaches 333 K. As expected, the narrowing process is accompanied by a change of the line shape from a Gaussian to a Lorentzian. At approximately 400 K the regime of extreme narrowing ($T \rightarrow \infty$) is reached where $\delta = \delta_\infty$ is solely determined by inhomogeneities of the external magnetic field. In that region, dipole-dipole interactions are completely averaged due to sufficiently fast Li diffusion, indicating an average jump rate on the order some tens of kHz in this temperature range.

In Fig. 4 the NMR line width δ is plotted as a function of temperature, exhibiting a typical motional narrowing (MN) curve. A few approaches can be found in the literature aiming at the analysis of $\delta(T)$ curves in order to estimate the activation energy of the underlying Li diffusion process. If the full $\delta(T)$ curve cannot be determined, the activation energy of the underlying Li hopping process can be estimated by using the empirical expression of Waugh and Fedin,[56]

$$E_a^{\mathrm{WF}} = 1.617 \times 10^{-3} \cdot T_c/\mathrm{K}, \tag{1}$$

where T_c, denotes the so-called onset temperature of MN. With $T_c \approx 290$ K, E_a^{WF} amounts to be approximately 0.47 eV, which is here in good agreement with the value probed by SLR NMR, as shown below. The dashed line in Fig. 4 shows a fit according to the *ad hoc* formalism introduced by Abragam[57] for motional averaging of dipole-dipole interactions:

$$\delta(T) = \sqrt{\delta_0^2 \frac{2}{\pi} \arctan\left[\varsigma \delta(T) \tau_{0\,\mathrm{MN}} \exp\left(\frac{E_a^{\mathrm{MN}}}{k_B T}\right)\right] + \delta_\infty^2}, \tag{2}$$

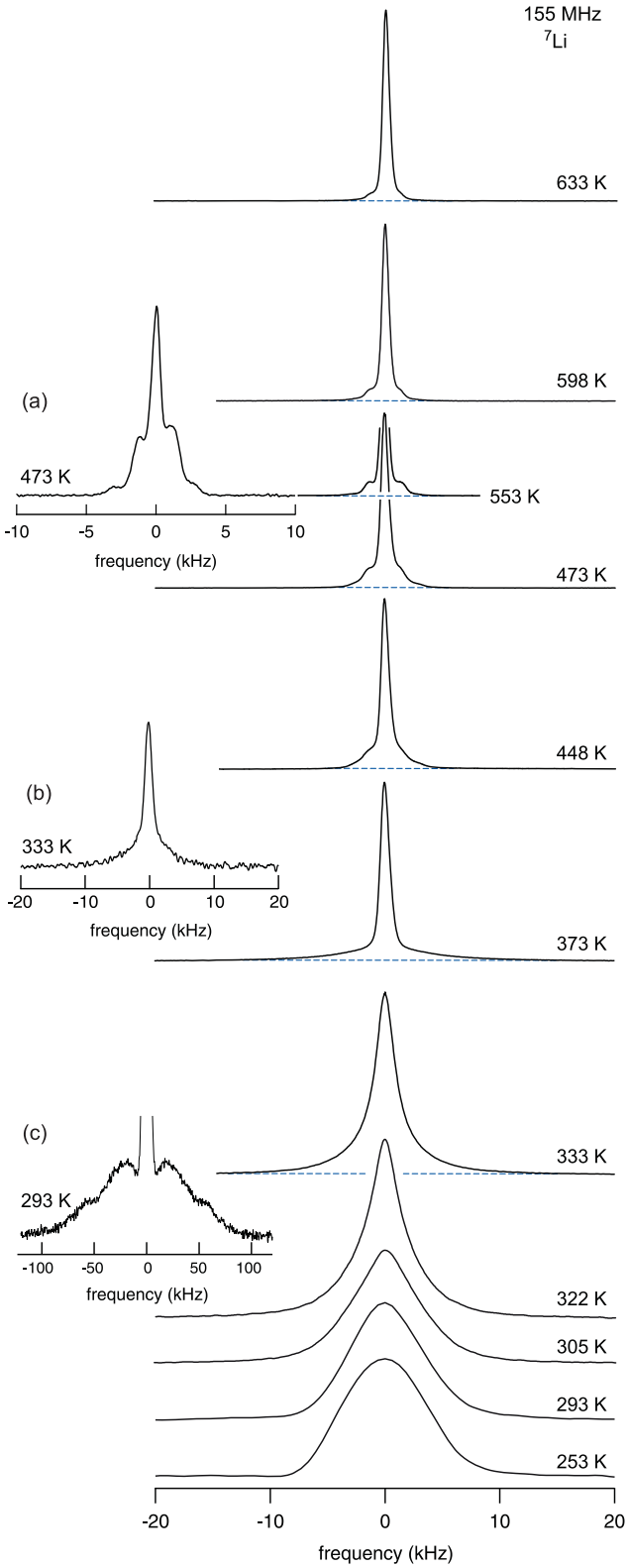

FIG. 3. Temperature-variable ^{7}Li NMR spectra of polycrystalline garnet-type $Li_7La_3Zr_2O_{12}$ recorded at a resonance frequency of 155 MHz. The spectra were obtained directly from the FIDs of the ^{7}Li SLR NMR measurements in the laboratory frame of reference. The insets (a), (b), and (c) represent NMR spectra obtained after Fourier transformation of ^{7}Li NMR spin-alignment echoes beginning from their top. See text for further details.

where ς is a fit parameter here chosen to be one. k_B denotes Boltzmann's constant and τ_0^{MN} represents the pre-exponential factor of the corresponding correlation time τ_c^{MN}. The activation energy E_a^{MN} turned out to be approximately 0.43 eV, thus underestimating the precise value E_a obtained from SLR NMR by approximately 10% (see below). The same activation energy is obtained when $\tau_c^{MN}(\delta)$ values are calculated and plotted vs the inverse temperature $1/T$ (see the inset of Fig. 4). However, analyzing the data according to the phenomenological equation of Hendrickson and Bray, which is given in Ref. 58, yields a much higher activation energy, although the resulting fit, which is not shown for the sake of clarity here, nearly coincides with that shown in Fig. 4. This difference clearly indicates that in some cases the extraction of quantitative information from temperature-variable line widths measurements is fraught with large difficulties. Even within a given approach these difficulties appear; the solid line in Fig. 4 represents an alternative fit according to Eq. (2), however, with the fit parameter E_a^{MN} being fixed at 0.5 eV. This is roughly the activation energy probed by impedance spectroscopy (see below). The very small differences of the two fits reveal that irrespective of the validity of these models for spin-3/2 nuclei, highly precise line width measurements are required to give accurate results. Obviously, small errors in measurement could have a large impact on the resulting parameters of interest.

Nevertheless, line-shape measurements are highly valuable for a rough estimate of diffusion parameters in ionically conducting solids.[32,33,59–63] Here, the results indicate that the maximum of the diffusion-induced ^{7}Li SLR NMR rate peak $[R_{1\varrho}(1/T)]$, when recorded at a locking frequency $\omega_1/2\pi$ in the kHz range, should show up between 300 K and 400 K. Indeed, this is exactly found for the garnet-type oxide studied here (see below).

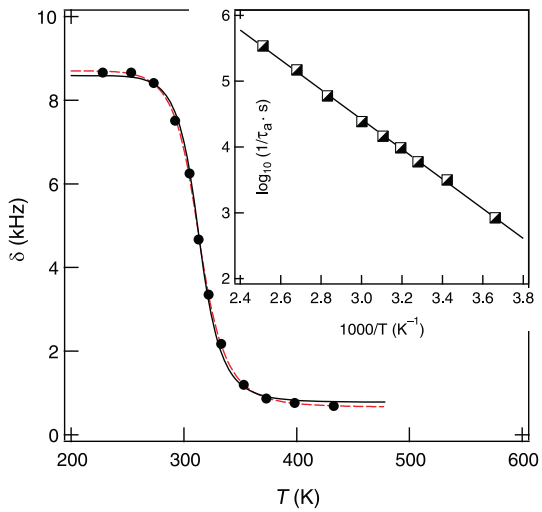

FIG. 4. (Color online) ^{7}Li NMR line widths δ of the central line versus temperature. The dashed line represents a fit according to Eq. (2) with no restrictions for the adjustable parameters. The solid line shows the same fit, however, with E_a being fixed at 0.5 eV. (Inset) Arrhenius plot of the correlation rates τ_a^{-1} of Eq. (2). The solid line shows a fit according to the corresponding Arrhenius relation and yields $E_a \approx 0.43$ eV.

2. ^{7}Li NMR spectra: Quadrupole intensities

In order to study the temperature behavior of the quadrupole intensities (see above), complete NMR spectra were recorded by using the stimulated echo technique. Exemplarily, in the insets of Fig. 3 ^{7}Li spin-alignment echo NMR spectra are shown which were acquired with the Jeener-Broekaert pulse sequence. Besides its central line, the room temperature ^{7}Li NMR spectrum of tetragonal $Li_7La_3Zr_2O_{12}$ exhibits a powder pattern of satellite intensities. In the tetragonal phase of $Li_7La_3Zr_2O_{12}$ the Li ions occupy distinct crystallographic sites being characterized by different electric field gradients. Most likely, the quadrupole intensity is composed of distinct patterns belonging to the Li ions residing on the distorted octahedral sites[13] (see above). However, distinct patterns are difficult to resolve because of dipole-dipole interactions broadening the spectrum. From the outer wings an average coupling constant C_q of approximately 108 kHz can be estimated.

At a sufficiently large Li jump rate, on the order of $\tau^{-1} \approx 10^5$ s^{-1}, quadrupole interactions are expected to be averaged to a great extent provided an isotropic diffusion process is present in which all Li sites participate equally. In fact, in the NMR spectrum recorded at 333 K (see inset (b) of Fig. 3) any significant contributions from quadrupole interactions are absent. However, as can be seen from the Fourier transforms of the FIDs in Fig. 3, a new quadrupole powder pattern emerges characterized by a much smaller coupling constant of $C_q' \approx 4.6$ kHz. This is more apparent in the stimulated echo NMR spectrum (inset (a) of Fig. 3). In general, in single-phase materials this reflects incomplete averaging of quadrupole couplings and indicates an anisotropic diffusion process; for comparison, see also Ref. 39. Here the change from tetragonal to cubic symmetry (see Ref. 37) might also be related to this observation. When the temperature is increased to 663 K the intensity of these residual satellite contributions finally decreases. At even higher temperatures a single NMR resonance is expected due to complete averaging. Most likely, besides the main diffusion process causing line narrowing, averaging of quadrupole interactions governing the spectrum at room temperature (inset (c) of Fig. 3) as well as NMR SLR (see below), the ions seem to get access to further diffusion pathways if the temperature is sufficiently high. However, owing to the small value of C_q' this additional process has to be characterized by a very small exchange rate since full averaging is not reached at 663 K yet. It might reflect Li exchange between the two spin reservoirs made visible in Fig. 2, which are also present in $Li_7La_3Zr_2O_{12}$ with cubic symmetry. While the majority of the Li ions in the octahedral interstices govern the diffusion properties of $Li_7La_3Zr_2O_{12}$, Li ions occupying tetrahedral sites take part in the diffusion process at higher temperatures only. However, the latter has a negligible influence on the overall jump rates measured below.

C. ^{7}Li NMR spin-lattice relaxation rates

1. Basics of ^{7}Li NMR spin-lattice relaxation

Within an NMR relaxation experiment the equilibrium state of a spin system exposed to an external magnetic field B_0 is perturbed in a specific way by a short external radio frequency pulse. Immediately after excitation the spin system will start to return to its state of thermal equilibrium. The recovery of longitudinal magnetization M_z, that is, the magnetization aligned with the external magnetic field, is called spin-lattice relaxation. This process can be recorded when the recovery of M_z along the axis z defined by the magnetic field B_0 is monitored as a function of waiting (or delay) time t. Usually, the transient $M_z(t)$ follows an exponential containing the temperature-dependent SLR NMR rate $R_1 = 1/T_1$ (or $R_{1\varrho} = 1/T_{1\varrho}$), being a measure of the transition probability of the spins between distinct Zeeman levels.

In general, if SLR is solely induced by diffusion processes, the rate $R_{1(\varrho)}$ is proportional to the spectral density function $J(\omega)$, which is the Fourier transform of the correlation function $G(t)$. $G(t)$ contains the temporal information of the atomic diffusion. It describes the internal fluctuating dipolar magnetic or quadrupolar electric fields due to the motion of the ions. Transitions between the energy levels of the spin system will be induced and SLR becomes effective, when $J(\omega)$ has components at the transition frequencies $\omega = \omega_0$ and $\omega = \omega_1$, respectively. The SLR NMR rates may be expressed in terms of the Lorentzian-shaped spectral density functions $J^{(q)}(\omega_{0(1)})$ given in, for example, Refs. 57 and 64:

$$R_1 \propto J^{(1)}(\omega_0) + J^{(2)}(2\omega_0), \tag{3}$$

$$R_{1\varrho} \propto J^{(0)}(2\omega_1) + 10J^{(1)}(\omega_0) + J^{(2)}(2\omega_0). \tag{4}$$

$J^{(q)}(\omega_{0(1)})$ with $q = 0, 1, 2$ denote spectral densities which result in transitions of spin pairs where the combined angular momentum changes by $q\hbar$. $\hbar$ is Planck's constant divided by 2π. The phenomenological SLR NMR model introduced by Bloembergen, Purcell, and Pound (BPP) considers random jump diffusion. The correlation function is assumed to be an exponential,[65]

$$G(t)^{(q)} = G^{(q)}(t = 0)\exp(-|t|/\tau_c), \tag{5}$$

leading to a Lorentzian-shaped spectral density function,

$$J^{(q)}(\omega) = G^{(q)}(t = 0)\frac{2\tau_c}{1 + (\omega\tau_c)^\beta} \text{ with } \beta = 2 \text{ (BPP)}. \tag{6}$$

The temperature dependence of the correlation time τ_c or the corresponding rate can be described by an Arrhenius relation,

$$\tau_c^{-1} = \tau_{c,0}^{-1}\exp[-E_a/(k_B T)]. \tag{7}$$

Altogether, the diffusion-induced relaxation rate R_1, measured at $\omega = \omega_0$ (or $\omega = \omega_1$), first increases with increasing T (low-T range, $\omega_0\tau \gg 1$), passes through a maximum at a specific temperature $T_{\max}$, and then decreases [high-T range, $\omega_0\tau \ll 1$)]. Taking into account the frequency dependence of $R_1(\omega_{0(\varrho)}, T)$, the behavior can be summarized as follows:

$$R_{1(\varrho)} \propto \begin{cases} \exp[E_{a\,\text{low}}/(k_B T))], & \text{if } T \gg T_{\max}, \\ \omega_{0(1)}^{\beta}\exp[-E_{a\,\text{high}}/(k_B T)], & \text{if } T \ll T_{\max}. \end{cases} \tag{8}$$

$T_{\max} = f(\omega_{0(\varrho)})$ decreases with decreasing Larmor and locking frequency, respectively. The absolute value of ω_0 is linked to the external homogenous magnetic field B_0 via $\omega_0 = \gamma B_0$, where γ is the magnetogyric ratio of the probe nucleus.

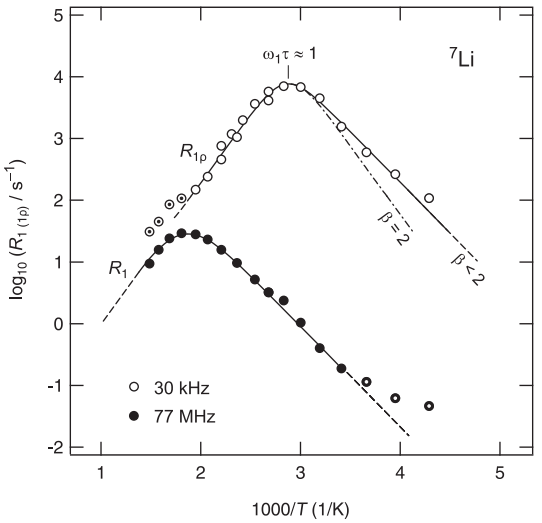

FIG. 5. ^{7}Li NMR SLR rates of garnet-type $Li_7La_3Zr_2O_{12}$ recorded in both the laboratory (•) and the rotating frame of reference (○). The solid lines show fits according to Eqs. (3) and (4). Data points marked with a dot were excluded from the fit (see text for further details). The dashed-dotted line illustrates the deviation of the rate peak $R_{1\varrho}(1/T)$ from simple BPP-type behavior characterized by $\beta = 2$.

Usually B_0 has a value of several teslas so that $\omega_0/2\pi$ is of the order of 100 MHz. At the temperature $T_{max}(\omega_0)$ where the rate maximum appears, the correlation rate τ_c^{-1}, which is within a factor of two identical with the mean Li jump rate τ^{-1}, is of the order of ω_0 meaning $\omega_0\tau_c \approx 1$. The temperature dependence of τ^{-1} is given by an Arrhenius relation being analogous to that of the correlation rate: $\tau^{-1} = \tau_0^{-1}\exp(-E_a/k_BT)$. Thus, SLR NMR measurements allow for the determination of extremely fast Li jump processes characterized by rates on the order of 10^9 s^{-1}. If the diffusion-induced maximum is recorded, $\tau^{-1}(1/T_{max})$ can be directly determined. Regarding SLR NMR measurements performed in the rotating frame of reference,[49,66] ω_0 has to be replaced with the locking frequency ω_1 and B_0 with the radio-frequency magnetic field B_1. The locking field B_1 corresponds to $\omega_1/2\pi$ values in the kHz range, making the method ideal for the detection of slower Li motions with jump rates on the order of 10^5 s^{-1}.

2. *Arrhenius plot of the ^{7}Li SLR NMR data and analysis of the diffusion-induced rate peaks*

^{7}Li SLR NMR rates of $Li_7La_3Zr_2O_{12}$ measured at $\omega_1/2\pi$ = 30 kHz as well as $\omega_0/2\pi = 77.8$ MHz are plotted in the Arrhenius diagram of Fig. 5. As indicated by the line widths analysis (see above), the rate maximum shows up at approximately $T_{max} = 325$ K and 530 K, respectively. The mean Li jump rates at these two temperatures turn out to be 1.9×10^5 s^{-1} and 4.9×10^8 s^{-1}, respectively. As expected, the SLR NMR rate peak recorded at $\omega_0/2\pi = 155.5$ MHz is slightly shifted to higher temperatures. While its shape equals that of the peak recorded at the lower field, the maximum shows up at 570 K. The jump rate can be easily converted into the self-diffusion coefficient D_{sd} by means of the Einstein-Smoluchowski equation. In the case of 3D diffusion D_{sd} is expressed by $D_{sd} = a^2/(6\tau)$, where a is the jump distance which can be identified with the average Li-Li distance.[13] With a being of the order of 2 Å the diffusion coefficient at $T_{max} = 325$ K amounts to 1.3×10^{-17} m^2 s^{-1} and increases to 3.3×10^{-14} m^2 s^{-1} when T is raised to 530 K.

Interestingly, an asymmetric rate peak $R_{1\varrho}(1/T)$ is obtained; that is, the slope of the low-temperature flank ($T <$ 330 K) is lower than that of the high-temperature side, leading to $E_{a\,low} < E_{a\,high}$. Analyzing just the data points on the flanks of this peak, the corresponding activation energies are $E_{a,low} = 0.32(3)$ eV [the same value is found for the $R_1(1/T)$ peak] and $E_{a,high} = 0.48(3)$ eV, respectively. Asymmetric rate peaks are predicted by several BPP-based relaxation models taking into account correlation effects such as Coulomb interactions and/or structural disorder.[21] In particular, this holds for amorphous (glassy) ion conductors with an irregularly formed, time-dependent potential landscape the ions are exposed to while diffusing. Li diffusion in such materials is governed by nonexponential correlation functions reflecting a distribution of jump rates (as well as activation barriers).[32,67,68] In general, in the regime $\tau_c\omega_1 \gg 1$, i.e., on the low-temperature side of $R_{1\varrho}(1/T)$, only few Li jumps are sampled in the time interval set by ω_1. Therefore, Li motions taking place on a shorter length scale mainly cause SLR in this temperature regime. This is in contrast to the situation on the high-temperature flank, where $\tau_c\omega_1 \ll 1$ holds (see above) and long-range Li diffusion parameters are probed, which reasonably implies $E_{a,low} < E_{a,high}$.

The asymmetry of a SLR NMR rate peak is taken into account in Eq. (6) when the exponent β is allowed to adopt values in the interval $1 < \beta \leqslant 2$.[21] The original BPP model, which has been developed for uncorrelated jump diffusion, contains a quadratic dependence of the SLR NMR rate on frequency [$\beta = 2$; see Eq. (6)], leading to symmetric rate peaks; that is, $E_{a\,low} = E_{a\,high} = E_a$. Solid lines in Fig. 5 represent fits according to Eqs. (3) and (4) for R_1 and $R_{1\varrho}$, respectively. The angular frequencies ω_0 and ω_1 were kept constant. The spectral density functions $J^{(q)}(\omega_{0(1)})$ are defined in Ref. 64 considering exponential correlation functions. The functions $J^{(q)}(\omega_{0(1)})$ are of the form of Eq. (6) taking into account $1 < \beta \leqslant 2$ leading to $R_{1(\varrho)} \propto \omega^\beta$ in the limit $\omega_{0(1)}\tau_c \ll 1$. On the high-temperature flank of the diffusion-induced rate peak the SLR rate is independent of frequency. In the case of $R_{1\varrho}$ NMR measurements the fit shown in Fig. 5 yields $E_a = 0.47(2)$ eV and $\beta = 1.7(1)$. The same parameters can be used to describe the R_1 peak. The results fulfill the relation $E_{a,low} = (\beta - 1) \cdot E_{a,high}$ given in Ref. 21. As an illustration the dashed-dotted line of Fig. 5 indicates the shape of $R_{1\varrho}(1/T)$ for uncorrelated motion. This means that it represents the behavior for $\beta = 2$ leading to a symmetric rate peak.

Let us mention that the data points marked by dots were excluded from the fits shown. The R_1 rates recorded below approximately 260 K are increasingly governed by nondiffusive background effects caused, for example, by lattice vibrations or coupling of the spins with paramagnetic impurities. Above 530 K the $R_{1\varrho}$ rates are already influenced by R_1 [see Eqs. (3) and (4)]. Hence, the measured rate turned out to be larger than expected without this contribution. It is roughly taken into account in the global fit shown below.

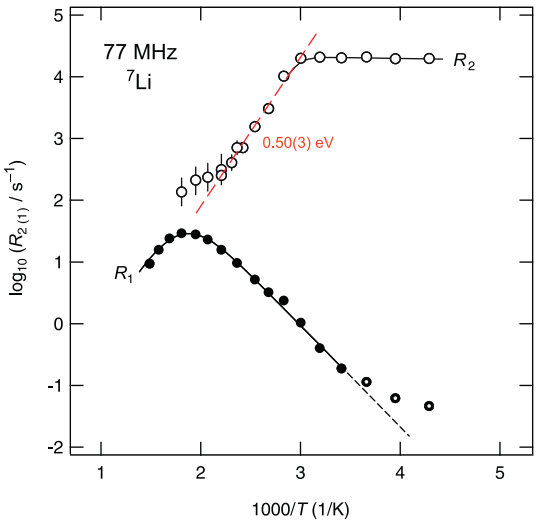

FIG. 6. (Color online) Temperature dependence of the ^{7}Li NMR SSR rates R_2 of $Li_7La_3Zr_2O_{12}$. The dashed line represents a fit according to an Arrhenius law yielding an activation energy of 0.50(3) eV. For comparison, the rates R_1 of Fig. 5 are shown, too.

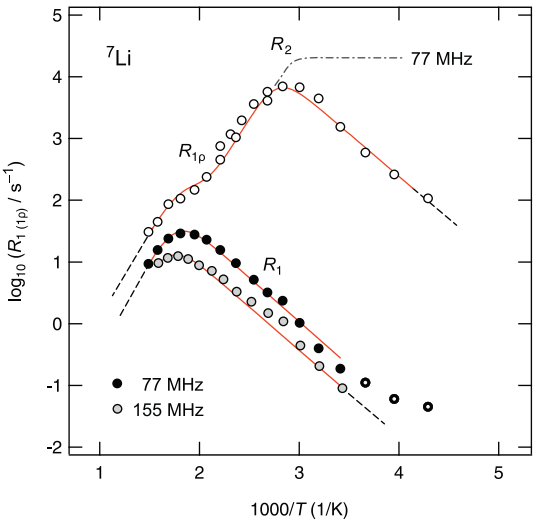

FIG. 7. (Color online) ^{7}Li NMR SLR rates R_1 as well as $R_{1\varrho}$ recorded at $\omega_1/2\pi = 30$ kHz and at 77 and 155 MHz. The solid lines represent a global fit according to Eqs. (3) and (4). The dashed-dotted line indicates the position of the SSR rates R_2 shown in Fig. 6. At higher T the R_2 rates follow the behavior of $R_{1\varrho}$. Note that the fitting functions were modified such that dipolar relaxation is taken into account (see text for further details). Furthermore, ω_1 was replaced by an effective locking frequency $\omega_{\rm eff}$ taking into account the coupling of the Li spins with paramagnetic centers. The data points marked by dots were excluded from the fit.

3. *Brief analysis of ^{7}Li spin-spin relaxation NMR rates*

Compared with $E_a = 0.47(2)$ eV obtained from SLR NMR performed in the rotating frame of reference, a very similar activation energy can be deduced from temperature-variable spin-spin relaxation (SSR) NMR rate measurements when the temperature regime of MN is analyzed. SSR NMR rates R_2, which were recorded at a resonance frequency of 77 MHz, are plotted in the Arrhenius diagram of Fig. 6. For comparison, the corresponding rates R_1 are shown, too. In terms of spectral densities $J^{(q)}$ the rate R_2, when governed by homonuclear dipole-dipole interactions, reads[21]

$$R_2 \propto J^{(0)}(0) + 10J^{(1)}(\omega_0) + J^{(2)}(2\omega_0). \tag{9}$$

If the Li jump rate τ^{-1} is much smaller than ω_0, the rate R_2 is approximately given by

$$R_2 \propto J^{(0)}(0) \propto \tau, \tag{10}$$

which holds for $J^{(0)}\tau \ll 1$ or $G^{(0)}\tau^2 \ll 1$ (MN regime; see above). This condition is violated at very low temperatures where $\tau^{-1} \ll R_2$ (rigid lattice), that is, in the limit $G^{(0)}\tau^2 \gg 1$. As mentioned above, the spins experience slightly different dipolar interactions, leading to a Gaussian distribution of frequencies around the mean value ω_0. The rigid-lattice result is given by $R_{20} = \sqrt{G^{(0)}} = \text{const}$. Here, $1/R_{20} = T_{20}$ turns out to be about 45 μs. In the present case Eq. (10) is valid in the temperature range from 300 K to 430 K. From the dashed line in Fig. 6 an activation energy of approximately 0.5 eV can be deduced, which is in good agreement with that probed by impedance spectroscopy (see below). As in the case of $R_{1\varrho}$, at much higher temperatures, that is, in the so-called extreme narrowing regime, $J^{(1)}(\omega_0)$ and $J^{(2)}(2\omega_0)$ increasingly start to contribute to transverse relaxation (see the deviations of the data points in Fig. 6 with respect to the dashed line).

4. *Global analysis of the NMR relaxation rates*

Careful inspection of the NMR rates shows that at the highest temperature, i.e., in the limit $\omega_0\tau \gg 1$, the ratio R_2/R_1 is approximately given by $R_2/R_1 \approx 4$. This is in good agreement with the prediction $R_2/R_1 = (I + 1/2)^2$ for (magnetic dipolar) coupling to paramagnetic impurities which is obtained for half-integer spins ($I > 1/2$) when only the central transition is regarded.[69] Such couplings are taken into account by the so-called global fit shown in Fig. 7, where all the fitting parameters of the three curves, that is, E_a, τ_0^{-1}, β, as well as the other prefactors, are linked to each other. In other words, a single diffusion process with a set of temperature-independent parameters is assumed.

The R_2/R_1 ratio is implemented in the fit by multiplying the respective $J^{(i)}(\omega_0)$ terms in Eq. (4) with a factor of four. It is important to note that a successful joint fit can only be obtained when ω_1 is replaced by an effective locking frequency $\omega_{\rm eff}$ taking into account local magnetic fields caused by paramagnetic impurities. Comparing the prefactor of Eq. (3) with that one deduced from the second moment yields $\omega_{\rm eff} \approx 2\omega_1$. The corresponding jump rate (see the above estimation using ω_1 instead of $\omega_{\rm eff}$) increases accordingly.

Taken together, the joint fit of Fig. 7, which also makes use of an exponent β with $1 < \beta \leqslant 2$ (see above), yields an activation energy of 0.54(4) which is slightly larger than that obtained by analyzing the rate peaks independently of each other (see Fig. 6). From the global fit a β value of 1.5(1) is obtained which might indicate that a nonexponential correlation function governs Li diffusion in the garnet. The

pre-exponential factor amounts to approximately $\tau_0^{-1} = 1.4 \times 10^{14}$ s^{-1}, which is in the typical range of phonon frequencies.

D. Comparison with results from impedance spectroscopy

For the comparison of Li jump rates deduced from SLR NMR with results from impedance data (presented in Fig. 8), the measured conductivity values σ' characterizing the bulk response of $Li_7La_3Zr_2O_{12}$ have been converted into jump rates τ^{-1}.

This has been done by means of the Nernst-Einstein and Einstein-Smoluchowski equations. The first one connects $\sigma' = f(T)$, which is the real part of the complex conductivity $\hat{\sigma}$, with the tracer diffusion coefficient D_{tr} via the Haven ratio H_{R},

$$D_{\mathrm{tr}} = H_{\mathrm{R}} \frac{\sigma' k_{\mathrm{B}} T}{N q^2}. \tag{11}$$

Here we have assumed $H_R = 1$. q in Eq. (11) represents the charge of the Li ions and N denotes the number density of charge carriers in the garnet. The macroscopic diffusion coefficient D_{tr} is related via the correlation factor f to the microscopic self-diffusion coefficient, $D_{\mathrm{tr}} = f D_{\mathrm{sd}}$. The correlation factor f reflects the degree of correlated motion of the charge carriers. It ranges between 0 and 1. $f = 1$ is obtained for uncorrelated motion. Using $D_{\mathrm{sd}} = a^2/(6\tau)$ (see above) τ^{-1} and σ' are connected to each other according to the following expression:

$$\tau^{-1} = H_{\mathrm{R}} f \frac{6 k_{\mathrm{B}} T}{N q^2 a^2} \cdot \sigma'. \tag{12}$$

Here σ' equals the so-called dc conductivity σ'_{dc} which is obtained when the conductivity, which is measured as a function frequency ν, is extrapolated to $\nu \to 0$. Figure 8(a) shows some typical impedance spectra $\sigma'(\nu)$, illustrating the difficulty to determine σ'_{dc} characterizing Li transport in the bulk of polycrystalline $Li_7La_3Zr_2O_{12}$ prepared as a powder sample. These difficulties arise from the presence of very pronounced blocking effects being caused by grain boundaries as well as metallic electrodes [Fig. 8(a)]. In the case of cold-pressed and nonsintered pellets these contributions dominate the impedance spectra at high temperatures and (or) low frequencies, in particular. Determination of ion conductivities using Cole-Cole plots is fraught with the same uncertainties. The different contributions of the electrical response can also be distinguished by plotting the real part of the capacity as a function of frequency. The bulk response is characterized by a capacitance of approximately 4 pF while those associated with grain boundary processes and electrode effects are in the order of 100 and 10^7 pF, respectively. In Fig. 9 the τ^{-1} rates calculated from the bulk σ'_{dc} values which were read out from the ac-conductivity isotherms shown in Fig. 8(a) (nonsintered pellet) are plotted versus the inverse temperature. For this estimation, we have simply assumed $f = 1$.

For a direct comparison with NMR results, the Li jump rates obtained from the diffusion-induced rate peaks are also included in Fig. 9. Note that in the case of $R_{1\varrho}$ the upper value is calculated using ω_{eff} while the other one simply by the use of ω_1. The data point labeled by MN corresponds to a Li jump rate estimated from the inflexion point of the MN curve shown in Fig. 4. At the corresponding temperature the jump rate can be estimated according to the relation $\tau^{-1} \approx 2\pi\delta_0$. The consistency of the absolute values shows that both methods obviously probe the same Li dynamics in $Li_7La_3Zr_2O_{12}$. While conductivity measurements can be regarded as a tool probing transport in a macroscopic way, SLR NMR spectroscopy is capable of measuring the same parameters from a microscopic, that is, atomic-scale point of view. It takes advantage of internal dipolar-magnetic as well as quadrupolar-electric field fluctuations caused by the diffusive motion of the spins. While NMR is sensitive to Li motions characterized by residence times of the order of the inverse Larmor or locking frequency given by $\omega_0^{-1} \approx 1$ ns and $\omega_1^{-1} \approx 1$ μs, respectively, σ'_{dc} values were measured in the frequency range from 0.1 s to 1 μs. Thus, SLR NMR performed in the rotating frame of reference as well as impedance spectroscopy probe Li jump rates on the same time scale, however, in a quite different manner. The solid line shown in Fig. 9 represents an Arrhenius fit using all the data points shown except the one at the lowest temperature. The so-called long-range activation energy, being relevant for the application of the material in lithium-ion batteries, turned out to be $E_a = 0.52(2)$ eV and the pre-exponential factor τ_0^{-1} is on the order of 1×10^{14} s^{-1}. The activation energy deduced is in good agreement with that one probed by analyzing the diffusion-controlled NMR relaxation rate peaks as well as temperature-variable NMR SSR rates. From the fit of Fig. 9 the room-temperature diffusion coefficient D_{sd} turned out to be 1.8×10^{-18} m^2 s^{-1}. Interestingly, the gradual transition from a tetragonal to a cubic phase[37] (see above) is hardly reflected by the data. Thus, slight local changes in the structure do not show a significant influence on the dynamic parameters governing Li hopping in highly pure garnet-type $Li_7La_3Zr_2O_{12}$.

In order to prove in another way that the low-frequency part of the impedance spectra shown in Fig. 8(a) is not related to bulk processes, the impedance pellet was annealed in air at high temperatures. Sintering the pellet at 1098 K (or 1148 K) leads to impedance spectra which are, particularly at low temperatures, increasingly dominated by the electrical response of the bulk material. Hence, σ'_{dc} can be easier read out from the ac-conductivity isotherms shown in Fig. 8(b). As expected, the bulk response remains nearly unaffected by this annealing process. Presumably, small differences might be explained by slight structural changes (see above), as well as a possible loss of lithium after the material was exposed to very high temperatures. Here the corresponding rates (or σ'_{dc} values) of the sintered material nearly coincide with those of the as-prepared sample. The results obtained from the latter, which was investigated by NMR, are shown in Fig. 9. At high frequencies and low temperatures the σ'_{dc} plateau reflecting bulk conductivity merges into the (frequency-dependent) dispersive regime of $\sigma'(\nu)$. Below approximately 135 K $\sigma'(\nu)$ becomes independent of temperature and tends to follow the power law $\sigma'(\nu) \propto \nu^s$. For structurally disordered materials the fractional exponent s takes values in the range from 0.5 to 0.8 in most cases (universal dynamic response).[70] Here, s turned out to be 0.77 at $T = 135$ K.

Finally, in the Arrhenius plot of Fig. 8(c) bulk ion conductivities of $Li_7La_3Zr_2O_{12}$ are shown. For comparison, the corresponding conductivity values of the low-frequency plateau of Fig. 8(a) are also included. At ambient temperature

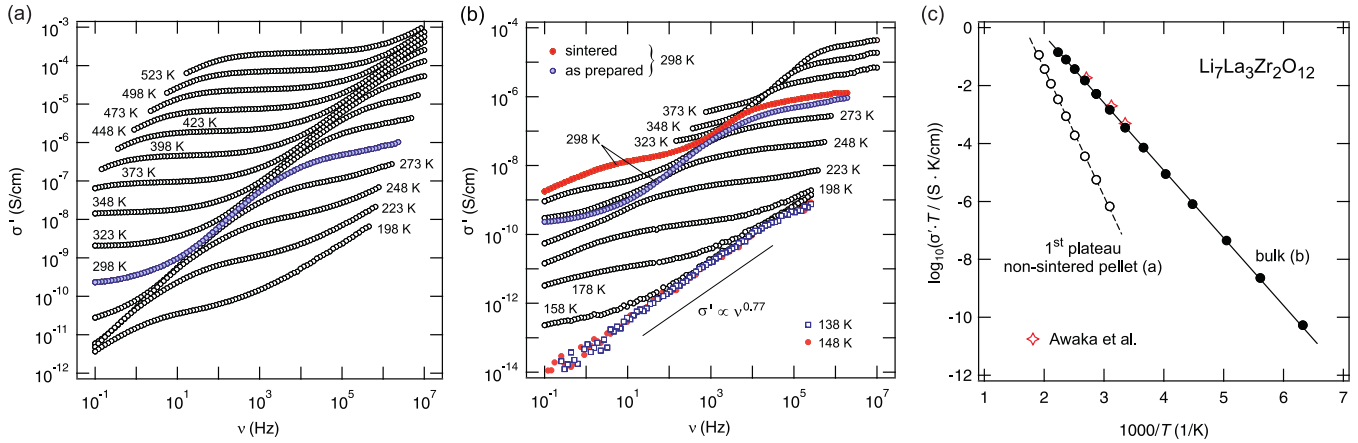

FIG. 8. (Color online) (a) Impedance spectra $\sigma'(\nu)$ of $Li_7La_3Zr_2O_{12}$ recorded at the temperatures indicated. The spectra are composed of different contributions reflecting electrode polarization, grain boundary, and bulk response (see, e.g., the highlighted spectra recorded at 298 K). The latter becomes most evident at low temperatures and merges into a dispersive regime at higher frequencies. σ'_{dc} of the bulk response is read out at the corresponding inflexion points. The uncertainty is somewhat less than half an order of magnitude (see also Fig. 9). At the lowest frequencies and highest temperatures, polarization effects showing up being characteristic for metallic electrodes blocking Li-ion transport. (b) Impedance spectra $\sigma'(\nu)$ of $Li_7La_3Zr_2O_{12}$ obtained after sintering the pellet at 1148 K. For comparison, the spectrum recorded at 298 K recorded before annealing is also shown. (c) σ'_{dc} (plotted as $\sigma'_{dc}T$ vs $1/T$) of the bulk response [see (b), sintered sample] as well as of the low-frequency conductivity plateau of the nonsintered sample [cf. panel (a)]. The solid line shows a fit according to $\sigma'_{dc}T \propto \exp[-E_a/(k_BT)]$, yielding $E_a = 0.47(2)$ eV (bulk). The dashed line corresponds to $E_a = 0.87(2)$ eV. For comparison, the data published recently by Awaka *et al.* are also shown (Ref. 13).

the lithium-ion dc conductivity of the bulk process is about 1.2×10^{-6} S cm^{-1}. This is in very good agreement with that one reported by Awaka *et al.*[13] The data follow an Arrhenius law characterized by an activation energy of approximately 0.46 eV. Almost the same value is probed by diffusion-induced ^{7}Li NMR SLR when the high-temperature flank of the diffusion-induced rate peak $R_{1\varrho}(1/T)$ is analyzed.

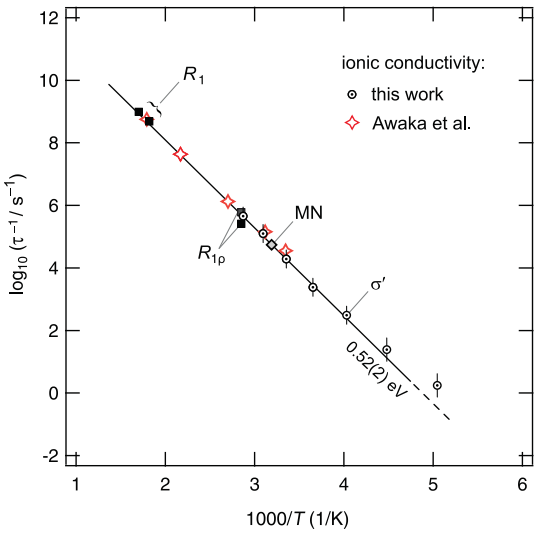

FIG. 9. (Color online) Temperature dependence of the Li jump rate in garnet-type $Li_7La_3Zr_2O_{12}$ as obtained from various NMR methods as well as ionic conductivity measurements. The jump rates deduced from R_1 NMR measurements were obtained at two different Larmor frequencies (see Sec. III C 1). For comparison, the conductivity data of Awaka *et al.* (Ref. 13), which were converted into Li jump rates according to Eq. (12), are also included. See Ref. 13 for details concerning these data points.

IV. CONCLUSIONS AND OUTLOOK

Polycrystalline garnet-type $Li_7La_3Zr_2O_{12}$, which was prepared by conventional solid-state synthesis, was investigated by temperature-variable NMR relaxation techniques particularly by monitoring purely diffusion-induced NMR SLR rate peaks in both the laboratory and the rotating frame of reference. While NMR line-shape measurements provide first insights into the Li dynamics in $Li_7La_3Zr_2O_{12}$, the fully recorded rate peak at a locking frequency of 30 kHz allowed, besides the observation of correlation effects, the precise and direct determination of Li self-diffusion parameters around ambient temperature. Altogether, the parameters characterizing Li dynamics, viz. jump rates and activation energies obtained by NMR, are in good agreement with those deduced from macroscopic conductivity measurements carried out in this study, as well as those reported in the literature quite recently. Let us note that the latter are often fraught with difficulties due to the unavoidable postpreparation of the sample specimens. In contrast, NMR is a noncontact method. Taken together, at ambient temperature the Li self-diffusion coefficient is in the order of 10^{-18} m^2 s^{-1}. Li hopping in the garnet structure is thermally activated characterized by $E_a \approx 0.5$ eV. Interestingly, when the tetragonal garnet is used as starting material, the smooth transformation to a cubic phase, whose structure is very similar to that of the tetragonal phase, has negligible influence on the Li jump rates deduced (see Fig. 9); their temperature behavior can be described by a single diffusion process. Thus, from a dynamic point of view the highly pure garnet-type $Li_7La_3Zr_2O_{12}$ investigated here acts like a single-phase material.

This is corroborated by recent NMR measurements in our laboratory. Ongoing NMR experiments of a monoclinic distorted $Li_7La_3Zr_2O_{12}$ does not show any significant

differences compared to the sample studied here. SLR NMR as well as frequency-dependent conductivity measurements on a sample, which was prepared such that it shows cubic symmetry at ambient temperature, are in progress in our laboratory. First results indicate that NMR SLR rates of a relatively pure, nonannealed sample are very similar to those presented in this work. Thus, slight structural changes seem to have no measurable influences on ion conductivity in the pure three-component system Li_2O:La_2O_3:ZrO_2. It has to be checked in detail what the origins are for the large increase in ion conductivity observed for a cubic sample of $Li_7La_3Zr_2O_{12}$ previously.[11] At least partially, it might be due to the incorporation of impurities such as Al cations, as proposed quite recently.[37]

ACKNOWLEDGMENTS

We thank Paul Heitjans (Hannover) for stimulating discussions as well as for access to his NMR laboratory in Hannover. We greatly acknowledge Konstanin Efimov and Armin Feldhoff (Hannover) for the *in situ* XRPD measurements carried out (at the last minute). We thank Frank Tietz (Forschungszentrum Jülich) for valuable discussions. Financial support by the Deutsche Forschungsgemeinschaft (DFG) in the framework of the Research unit FOR 1277 (Grant No. WI3600/2-1 and 4-1) as well as the Leibniz University Hannover ("Wege in die Forschung II") are highly appreciated.

*Author to whom correspondence should be addressed: wilkening@pci.uni-hannover.de

[1] A. V. Chadwick, Phys. Status Solidi A **204**, 631 (2007).

[2] P. Knauth and J. Schoonman (editors), *Nanocomposites—Ionic Conducting Materials and Structural Spectroscopies* (Springer, New York, 2007).

[3] H. L. Tuller, in *Springer Handbook of Electronic and Photonic Materials*, edited by S. Kasap and P. Capper (Springer, Berlin, 2006), Chap. 11, p. 213.

[4] S. Hull, Rep. Prog. Phys. **67**, 1233 (2004).

[5] E. Kendrick and P. Slater, Annu. Rep. Prog. Chem., Sect. A: Inorg. Chem. **106**, 429 (2010).

[6] A. S. Aricó, P. G. Bruce, B. Scrosati, J.-M. Tarascon, and W. V. Schalkwijk, Nature (London) **4**, 366 (2005).

[7] P. G. Bruce, B. Scrosati, and J.-M. Tarascon, Angew. Chem. Int. Ed. Engl. **47**, 2930 (2008).

[8] M. Whittingham, Chem. Rev. **104**, 4271 (2004).

[9] E. J. Cussen, J. Mater. Chem. **20**, 5167 (2010).

[10] A. Ramzy and V. Thangadurai, ACS Appl. Mater. Interfaces **2**, 385 (2010).

[11] R. Murugan, V. Thangadurai, and W. Weppner, Angew. Chem. Intern. Ed. **46**, 7778 (2007).

[12] M. Kotobuki, H. Munakata, K. Kanamura, Y. Sato, and T. Yoshida, J. Electrochem. Soc. **157**, A1076 (2010).

[13] J. Awaka, N. Kijima, H. Hayakawa, and J. Akimoto, J. Solid State Chem. **182**, 2046 (2009).

[14] V. Thangadurai, S. Adams, and W. Weppner, Chem. Mater. **16**, 2998 (2004).

[15] V. Thangadurai and W. Weppner, J. Am. Ceram. Soc. **88**, 411 (2005).

[16] V. Thangadurai and W. Weppner, Adv. Funct. Mater. **15**, 107 (2005).

[17] R. Murugan, W. Weppner, P. Schmid-Beurmann, and V. Thangadurai, Mater. Res. Bull. **43**, 2579 (2008).

[18] V. Thangadurai and W. Weppner, J. Power Sources **142**, 339 (2005).

[19] V. Thangadurai, H. Kaack, and W. Weppner, J. Am. Ceram. Soc. **86**, 437 (2003).

[20] R. Böhmer, K. Jeffrey, and M. Vogel, Prog. Nucl. Magn. Reson. Spectrosc. **50**, 87 (2007).

[21] P. Heitjans, A. Schirmer, and S. Indris, in *Diffusion in Condensed Matter—Methods, Materials, Models*, edited by P. Heitjans and J. Kärger (Springer, Berlin, 2005), Chap. 9, p. 369.

[22] L. S. Cahill, R. Chapman, J. Britten, and G. Goward, J. Phys. Chem. B **110**, 7171 (2006).

[23] L. J. M. Davis, I. Heinmaa, and G. R. Goward, Chem. Mater. **22**, 769 (2010).

[24] M. Wilkening and P. Heitjans, J. Phys. Condens. Matter **18**, 9849 (2006).

[25] M. Wilkening and P. Heitjans, Solid State Ionics **177**, 3031 (2006).

[26] Z. Xu and J. F. Stebbins, Science **270**, 1332 (1995).

[27] V. W. J. Verhoeven, I. M. de Schepper, G. Nachtegaal, A. P. M. Kentgens, E. M. Kelder, J. Schoonman, and F. M. Mulder, Phys. Rev. Lett. **86**, 4314 (2001).

[28] J. Cabana, N. Dupré, G. Rousse, C. P. Grey, and M. R. Palacin, Solid State Ion. **176**, 2205 (2005).

[29] M. Wilkening, W. Küchler, and P. Heitjans, Phys. Rev. Lett. **97**, 065901 (2006).

[30] M. Wilkening and P. Heitjans, Phys. Rev. B **77**, 024311 (2008).

[31] M. Wilkening, D. Gebauer, and P. Heitjans, J. Phys. Condens. Matter **20**, 022201 (2008).

[32] M. Wilkening, A. Kuhn, and P. Heitjans, Phys. Rev. B **78**, 054303 (2008).

[33] L. van Wüllen, T. Echelmeyer, H.-W. Meyer, and D. Wilmer, Phys. Chem. Chem. Phys. **9**, 3298 (2007).

[34] B. Koch and M. Vogel, Solid State Nucl. Magn. Reson. **34**, 37 (2008).

[35] M. Nyman, T. M. Alam, S. K. McIntyre, G. C. Bleier, and D. Ingersoll, Chem. Mater. **22**, 5401 (2010).

[36] M. P. O'Callaghan, A. S. Powell, J. J. Titman, G. Z. Chen, and E. J. Cussen, Chem. Mater. **20**, 2360 (2008).

[37] C. A. Geiger, E. Alekseev, B. Lazic, M. Fisch, T. Armbruster, R. Langner, M. Fechtelkord, N. Kim, T. Pettke, and W. Weppner, Inorg. Chem. **50**, 1089 (2011).

[38] D. Brinkmann, Prog. Nucl. Magn. Reson. Spectrosc. **24**, 527 (1992).

[39] R. Bertermann and W. Müller-Wahrmuth, Z. Naturforsch. **53a**, 863 (1998).

[40] J. Emery, J. Buzare, O. Bohnke, and J. Fourquet, Solid State Ionics **99**, 41 (1997).

[41] A. Rivera and J. Sanz, Phys. Rev. B **70**, 094301 (2004).

[42] C. León, M. L. Lucía, J. Santamaría, M. A. París, J. Sanz, and A. Várez, Phys. Rev. B **54**, 184 (1996).

[43] V. Epp and M. Wilkening, Phys. Rev. B **82**, 020301 (2010).

[44] M. Wilkening, W. Iwaniak, J. Heine, V. Epp, A. Kleinert, M. Behrens, G. Nuspl, W. Bensch, and P. Heitjans, Phys. Chem. Chem. Phys. **9**, 6199 (2007).

[45] D. Bork and P. Heitjans, J. Phys. Chem. B **105**, 9162 (2001).

[46] A. R. Allnatt and A. B. Lidiard, *Atomic Transport in Solids* (Cambridge University Press, Cambridge, 1993).

[47]H. Mehrer, *Diffusion in Solids* (Springer, Berlin, 2006).
[48]M. Wilkening, C. Mühle, M. Jansen, and P. Heitjans, J. Phys. Chem. B **111**, 8691 (2007).
[49]E. Fukushima and S. Roeder, *Experimental Pulse NMR* (Addison-Wesley, Reading, 1981).
[50]F. Qi, T. Jörg, and R. Böhmer, Solid State Nucl. Magn. Reson. **22**, 484 (2002).
[51]R. Böhmer, T. Jörg, F. Qi, and A. Titze, Chem. Phys. Lett. **316**, 419 (2000).
[52]F. Qi, C. Rier, R. Böhmer, W. Franke, and P. Heitjans, Phys. Rev. B **72**, 104301 (2005).
[53]X.-P. Tang and Y. Wu, J. Magn. Res. **133**, 155 (1998).
[54]Let us note that $Li_7La_3Zr_2O_{12}$, which was prepared such that it crystallizes with cubic symmetry already at room temperature, shows the same NMR spectral features as observed for the tetragonal modification here.
[55]T. Pietrass, F. Taulelle, P. Lavela, J. OlivierFourcade, J. Jumas, and S. Steuernagel, J. Phys. Chem. B **101**, 6715 (1997).
[56]J. Waugh and E. Fedin, Sov. Phys. Solid State **4**, 1633 (1963).
[57]A. Abragam, *The Principles of Nuclear Magnetism* (Clarendon, Oxford, 1961).
[58]J. Hendrickson and P. Bray, J. Magn. Res. **9**, 341 (1973).
[59]P. Heitjans, M. Masoud, A. Feldhoff, and M. Wilkening, Faraday Discuss. **134**, 67 (2007).
[60]K. Nakamura, H. Ohno, K. Okamura, Y. Michihiro, T. Moriga, I. Nakabayashi, and T. Kanashiro, Solid State Ionics **177**, 821 (2006).
[61]T. Matsuo, M. Shibasaki, and T. Katsumata, Solid State Ionics **154**, 759 (2002).
[62]H. Mattfeld, G. Balzer-Jöllenbeck, G. Meyer, and P. Heitjans, Solid State Ionics **62**, 265 (1993).
[63]Y. Xia, N. Machida, X. Wu, C. Lakeman, L. vanWullen, F. Lange, C. Levi, and H. Eckert, J. Phys. Chem. B **101**, 9180 (1997).
[64]C. A. Sholl, J. Phys. C: Solid State Phys. **14**, 447 (1981).
[65]N. Bloembergen, E. Purcell, and R. Pound, Phys. Rev. **73**, 679 (1948).
[66]D. C. Ailion and C. P. Slichter, Phys. Rev. **137**, A235 (1965).
[67]S. Faske, H. Eckert, and M. Vogel, Phys. Rev. B **77**, 104301 (2008).
[68]C. Brinkmann, S. Faske, B. Koch, and M. Vogel, Z. Phys. Chem. **224**, 1535 (2010).
[69]P. M. Richards, in *Topics in Current Physics*, edited by M. B. Salamon (Springer, Berlin, 1979), Vol. 15.
[70]K. Funke, C. Cramer, and D. Wilmer, in *Diffusion in Condensed Matter—Methods, Materials, Models*, edited by P. Heitjans and J. Kärger (Springer, Berlin, 2005), Chap. 9, p. 857.